Research Article | Vol. 29, No. 19 / 13 Sep 2021 / Optics Express 29982
Optics EXPRESS

Design guidelines for collimating or focusing graded-index fiber tips

NICOLAS RIESEN,[1,2,3,5,*] NICHOLAS PHILLIPS,[1,4,5] AND DAVID G. LANCASTER[1,2]

[1] *Future Industries Institute, STEM, University of South Australia, Mawson Lakes, SA 5095, Australia*
[2] *ARC Research Hub for Integrated Devices for End-user Analysis at Low-levels (IDEAL), Future Industries Institute, STEM, University of South Australia, Mawson Lakes, SA 5095, Australia*
[3] *Institute for Photonics and Advanced Sensing, University of Adelaide, SA 5005, Australia*
[4] *Defence Science and Technology Group, Third Ave, Edinburgh, SA 5111, Australia*
[5] *Authors contributed equally to this work*
[*] *nicolas.riesen@unisa.edu.au*

Abstract: Graded-index optical fiber probes suitable for focusing or collimating the output of an optical fiber at a wavelength of 1.3 µm have become an enabling technology in optical coherence tomography imaging applications for in vivo bioimaging. Such fiber tips however remain uncommon in other photonics applications. This paper provides the first numerical study of graded-index fiber tips covering a broad range of wavelengths spanning from the UV to short-infrared. The wavelength dependency and the influence of probe geometry on performance characteristics such as far-field divergence angle, spot size and working distance are analyzed. The paper yields easily accessible design guidelines for the fabrication of collimating or focusing fiber tips. Fiber collimators have considerable potential for use in free-space systems and could benefit a range of devices such as variable attenuators, dynamic wavelength equalisers and large 3D optical cross-connect switches, whereas focusing fiber tips have applications in high-resolution imaging.

1. Introduction

During the last two decades graded-index focusing or collimating fiber (GIF) tips have become an enabling technology in optical coherence tomography (OCT) for *in vivo* imaging within the human body [1–3]. Swanson *et al.* first proposed the design of such all-fiber ultra-small probes for compact OCT systems back in 2002 [4]. These probes were then demonstrated for OCT in 2005 by groups such as Jafri *et al.* [5] and have since been used for clinical delivery to deep-tissue locations using hypodermic needles or catheters for minimally invasive biomedical imaging. Amongst the many existing types of focusing or collimating devices and probes, fiber lenses such as those used in OCT have significant advantages in terms of small size, auto-alignment with fiber during splicing, mechanical strength and low back reflections [1]. Although some studies exist on fiber ball or hemispherical fiber lenses formed using melting or etching, GIF tip lenses have gained considerably more interest due to their versatility in terms of tuning the beam divergence angle, spot size and/or focal length [6].

Despite GIF tips having seen widespread use in OCT imaging typically at a wavelength of 1.3 µm [1,7–11], they remain uncommon outside of this specific application and wavelength. Note that GIF tips have also found some use in enhancing the fringe visibility of fiber-optic Fabry-Perot interferometers [12–14] for vibration [15,16] and temperature sensing [17]. They have also found some use in absorption spectroscopy [18]. The limited use of GIF tips in photonics applications is interesting since such probes have significant potential for a wide range of applications where optical collimation or focusing is important for fiber to free-space interfacing. Back-to-back or self-imaging arrangements of fiber collimators could for instance

#433541 https://doi.org/10.1364/OE.433541
Journal © 2021 Received 16 Jun 2021; revised 16 Aug 2021; accepted 17 Aug 2021; published 1 Sep 2021

Optics EXPRESS

be used in SMF-coupled free-space systems without the necessity for bulk optics. Coupling to free-space systems could benefit a range of devices including variable attenuators, dynamic wavelength equalisers and large 3D optical cross-connect switches [10]. These fiber lenses also have potential for use as mode field adaptors [19] and optical tweezers [20]. They could also be used to greatly reduce the numerical aperture (NA) of small-core fibers potentially avoiding the requirement for expensive high NA lenses in fiber to free-space applications. Whilst there are plenty of numerical and theoretical works at near-infrared wavelengths in the literature focusing on fiber-tip based OCT bioimaging [1–4,6–9,11,19,21–30], if GIF tips are to be used for more diverse photonics applications at a range of different wavelengths, a more comprehensive study of these collimating tips is needed. This article provides these studies, reporting on several design criteria and guidelines for the use of GIF tips at wavelengths ranging from the UV to short-infrared.

2. Background to GIF probes

2.1. Structure of GIF probes

The GIF tip or probe in its most versatile form consists of three fiber sections spliced together as shown in Fig. 1. The incoming fiber is usually standard single-mode fiber (SMF), followed by a section of coreless fiber (CF) which serves to expand the beam. The beam then enters a section of graded-index fiber which collimates or self-focuses the beam depending on its length.

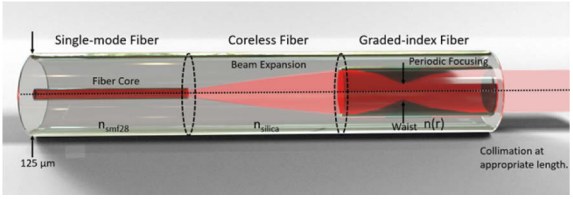

Fig. 1. Schematic of a GIF tip lens.

The graded-index fiber used has a parabolic refractive index profile that can be given as [1]:

$$n(r,\lambda) = \begin{cases} n_1(\lambda)\left(1 - \frac{g^2}{2}r^2\right) & r<a \\ n_2(\lambda) = n_{silica}(\lambda) & r \geq a \end{cases} \quad (1)$$

where n_1 is the peak refractive index, g is the gradient constant given by the manufacturer and a is the core radius. In this paper we assume Thorlabs GIF625 fiber for the graded-index fiber.

As discussed in this article the lengths of the CF and graded-index fiber are critical to the performance of the GIF tip [1]. This article provides design guidelines for low divergence angle collimating fiber tips as a function of the coreless and graded-index fiber lengths. We also provide design guidelines for imaging probes that maximize the NA for enhanced imaging resolution or increase the focal length for enhanced working distance. The studies presented extend on previous works [26,31], where spot size, divergence angle and working distance comparisons were made for GIF probes at specific wavelengths in the near infrared using simplified matrix methods. Such matrix methods (geometric optics approach) [26,31], are however not ideally suited to wavelength-dependence studies which are more effectively undertaken using the highly-accurate numerical beam propagation method (wave-optics approach) [13,18,32].

2.2. Setup and assumptions

This article demonstrates the influence of the coreless and graded-index fiber lengths on collimating or focusing performance and spot size of GIF tips. For the simulations standard

Optics EXPRESS

single-mode fiber was assumed (i.e. Corning SMF-28, index profile taken from [33]), whereas the CF was pure silica. The graded-index fiber simulated was Thorlabs GIF625, with the measured refractive index profile used for the simulations given in Fig. 2. The refractive index profile was measured with an IFA-100 refractive index profiler. Given that a broad range of wavelengths were simulated, material dispersion was accounted for using the appropriate Sellmeier equations for the different fiber segments. The modes of the SMF-28 fiber were numerically solved using RSOFT's FemSIM [34].

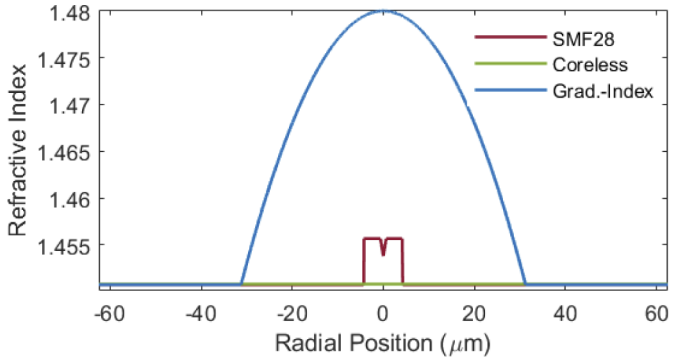

Fig. 2. Refractive index profiles of SMF-28 ([33], red trace), Thorlabs FG125LA coreless (measured, green trace) and graded-index GIF625 (measured, blue trace) fibers at 976 nm.

The propagation of the SMF-28 fiber modes through the GIF tips was simulated using the beam propagation method (BPM) via RSOFT BeamPROP (Version 2019.09) [13,18,32,35s]. BPM is an effective and highly-accurate wave optics tool to model light propagation in optic and photonic devices. For a given wavelength, a series of 2D BPM (x,z) propagation plots were generated as a function of coreless fiber (<400 μm) and graded-index fiber (<500 μm) lengths using the RSOFT MOST scan feature. Increments of 10 μm for each length parameter were chosen as this roughly represents the fabrication tolerances of such devices [13]. Each simulation for a given coreless and graded-index fiber length, yielded a single 2D contour plot (0.04 μm and 0.25 μm resolution in transverse and propagation directions, respectively) of the beam propagating through and from the device, from which the 1/e field radius was calculated along the propagation direction. We note that the refractive index in the axial z-direction does not change except at the interfaces of the device (where a finer mesh grid resolution was used, 0.04 μm). Hence the resolution in the axial z-direction was set lower than the resolution in the transverse x-direction. The axial length is also significantly larger than the transverse length. These settings were chosen to significantly reduce the overall simulation time without sacrificing accuracy. The simulation length was up to 5,000 μm to ensure far-field convergence. Note that the field diameter at the end of the coreless fiber can in principle exceed the core diameter of the graded-index fiber (62.5 μm) with long coreless fiber lengths. There is no value in extending the length of the coreless fiber beyond this effective expansion length. Therefore the field diameter of the beam in the coreless fiber was estimated using Gaussian optics and in particular the Rayleigh range to confirm that the coreless lengths were below the effective expansion length for all simulations [9,26].

The simulations were performed at typical laser wavelengths of 405 nm, 532 nm, 633 nm, 976 nm, 1310 nm, 1550 nm and 2100 nm. The total number of BPM simulations performed was 22,695 taking approximately 20 hours (~5 seconds per simulation) to complete when using a sequential script. For each BPM contour plot several parameters were extracted including the beam diameter at the fiber end-face (i.e. spot size), working distance (if focusing occurs) and the far-field divergence angle. The methods used to calculate these parameters are explained later on. The data was then collated to produce contour plots with the coreless and graded-index fiber

Optics EXPRESS

lengths as the dependent variables. An example of such data is given in Fig. 3, where the spot size (i.e. 1/e field diameter at the fiber end-face) and the far-field divergence angle at 633 nm is shown as functions of coreless and graded-index fiber lengths.

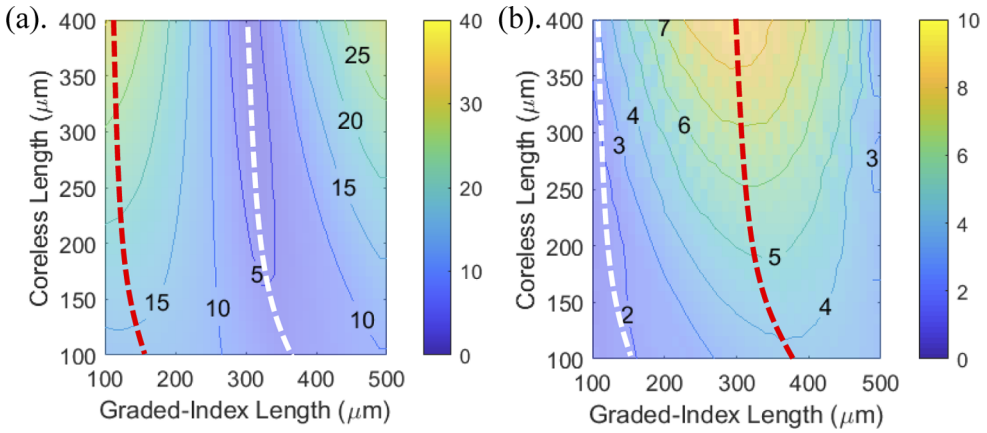

Fig. 3. Simulation of (a) 1/e field diameter (microns) at fiber end face and (b) far-field divergence angle (FFDA) in degrees, both at a wavelength of 633 nm.

As seen from Fig. 3(a) the region of minimum spot size at the end of the fiber (white dashed line) approximately coincides with the region of maximum FFDA (red dashed line) in Fig. 3(b). Similarly, the region of maximum spot size coincides with the region of minimum FFDA. This might be expected given that for a gaussian beam the FFDA is inversely proportional to the beam waist. Thus, a strongly focused beam will naturally diverge more whereas collimation is more likely for a larger beam size.

Such graphs could be used for extracting the optimal lengths of the graded-index and coreless fibers when fabricating collimating tips for the given wavelength. Note that a periodicity in the behavior of the GIF tips as a function of graded-index fiber length was observed as might be expected. The length of the graded-index fiber can be increased by half its pitch $P_L=2\pi/g$ or multiples thereof with no significant effect on performance. Note also that ripples in the plots were observed due to multimode interference. In the following section a broader wavelength-dependence study is provided.

2.3. Design guidelines for UV to short-infrared

As mentioned at each wavelength BPM simulations were performed for a range of coreless and graded-index fiber lengths with a step size of 10 μm. Greater resolution was not required due to the challenges of fabricating probes with such low dimensional tolerances. The wavelengths were 405 nm, 532 nm, 633 nm, 760 nm, 976 nm, 1310 nm, 1550 nm and 2100 nm.

2.3.1. Fiber spot size (1/e field diameter at end-face)

Figures 4 and 5 show the 1/e field diameter at the fiber end face as a function of coreless and graded-index fiber lengths. These values are directly extracted from the 1/e field radius output of BeamPROP at the end face of the probe.

Figure 4 shows that for a given GIF tip geometry, in general the shorter the wavelength the smaller the spot size as expected from the stronger confinement of light in the fiber segments at shorter wavelengths. This trend is also seen in Fig. 5. It is also observed that the trough in spot size shifts towards longer graded-index fiber lengths for a given coreless fiber length as the wavelength increases. It is also interesting to note that the dependency of the spot size on

Optics EXPRESS

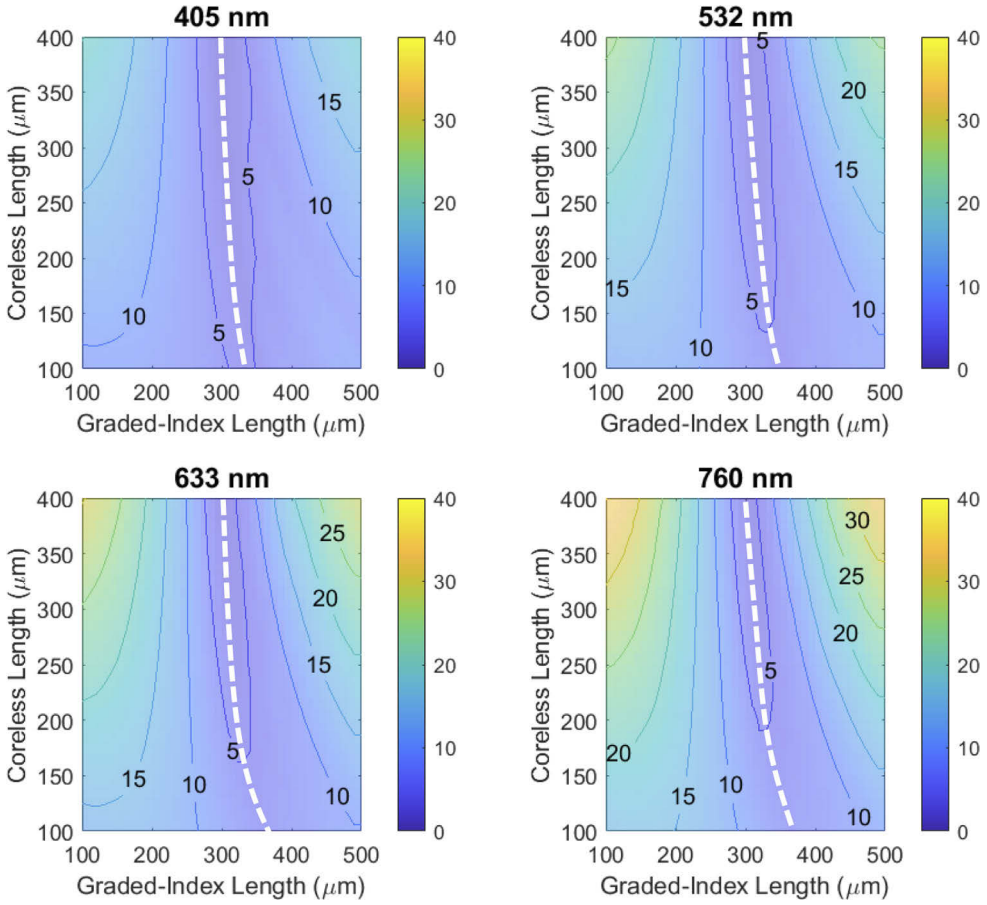

Fig. 4. The 1/e field diameter (microns) at the GIF tip end face as a function of coreless and graded-index fiber lengths. Results shown for wavelengths ranging from 405-760 nm.

GIF tip geometry increases as the wavelength increases. This is essentially due to the reduced confinement of light at longer wavelengths which in turn increases the focusing strength and sensitivity of the graded-index fiber segment.

In the simulations within this article only the fundamental mode is launched in the single-mode fiber. Whilst SMF-28 is few-mode in the visible, in practice single-mode performance can be achieved with careful launch conditions, mode strippers or mode-selective couplers [36]. The presence of more modes typically increases the spot size at the fiber end-face and also increases the far-field divergence angle. We note here that modelling of the 1/e field diameter is particularly useful for the design of mode field adapters and for the design of probes for various imaging applications.

2.3.2. Far-field divergence angle (FFDA)

The far-field divergence angle (FFDA) as a function of coreless and graded-index fiber lengths for the wavelengths considered is shown in Figs. 6 and 7. The far-field divergence angle (i.e. half-angle) was computed by applying a linear fit to the diverging beam. A linear section towards the end of the propagation path length in the far-field was selected using a threshold based on a second derivative of the 1/e field as a function of propagation distance. The far-field divergence angle plots provide critical results for the optimization of collimating tips.

Optics EXPRESS

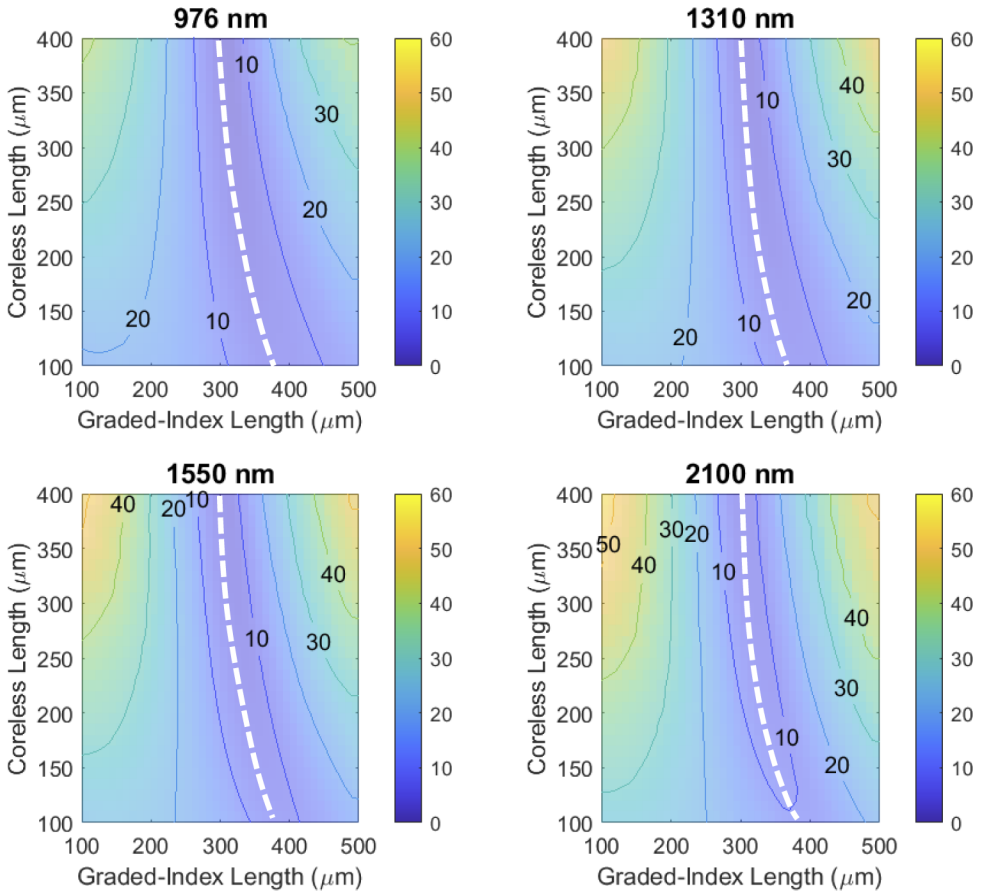

Fig. 5. The 1/e field diameter (microns) at the GIF tip end face as a function of coreless and graded-index fiber lengths. Results shown for wavelengths ranging from 976-2100 nm.

Figures 6 and 7 demonstrate that the far-field divergence angle (i.e. half-angle) is typically more sensitive to changes in geometry for longer wavelengths. This is likely due to the reduced confinement of light in the fiber cores, resulting in the light interacting with more of the graded-index profile increasing its focusing strength. Far-field divergence angles as small as $< 1°$ are observed along the white-dashed lines representing the troughs. The smallest possible divergence angle varies by only 1° between 405 and 2100 nm. We also note that the troughs tend towards longer graded-index fiber lengths for a given coreless length as the wavelength increases – especially for shorter coreless fiber lengths. On the other hand, if the coreless fiber is too short the beam will not expand sufficiently for the graded-index fiber to have full effect.

These far-field divergence angle contour plots provide easy-to-use guidelines for the design of collimating GIF tips. They also demonstrate how the performance of the GIF tip is very sensitive to small variations in the coreless fiber since it affects how the light enters the graded-index fiber section [26]. An example of typical beam divergence profiles used to calculate the FFDAs is shown in Fig. 8 for the case of a 100-micron graded-index fiber length and various different coreless fiber lengths. The simulation is at a wavelength of 976 nm.

This graph demonstrates the influence of coreless fiber length on focusing performance of the graded-index fiber segment. For longer lengths of coreless fiber which correspond to a larger beam interacting with the graded-index fiber, the focusing strength of the probe increases. Clearly

Optics EXPRESS

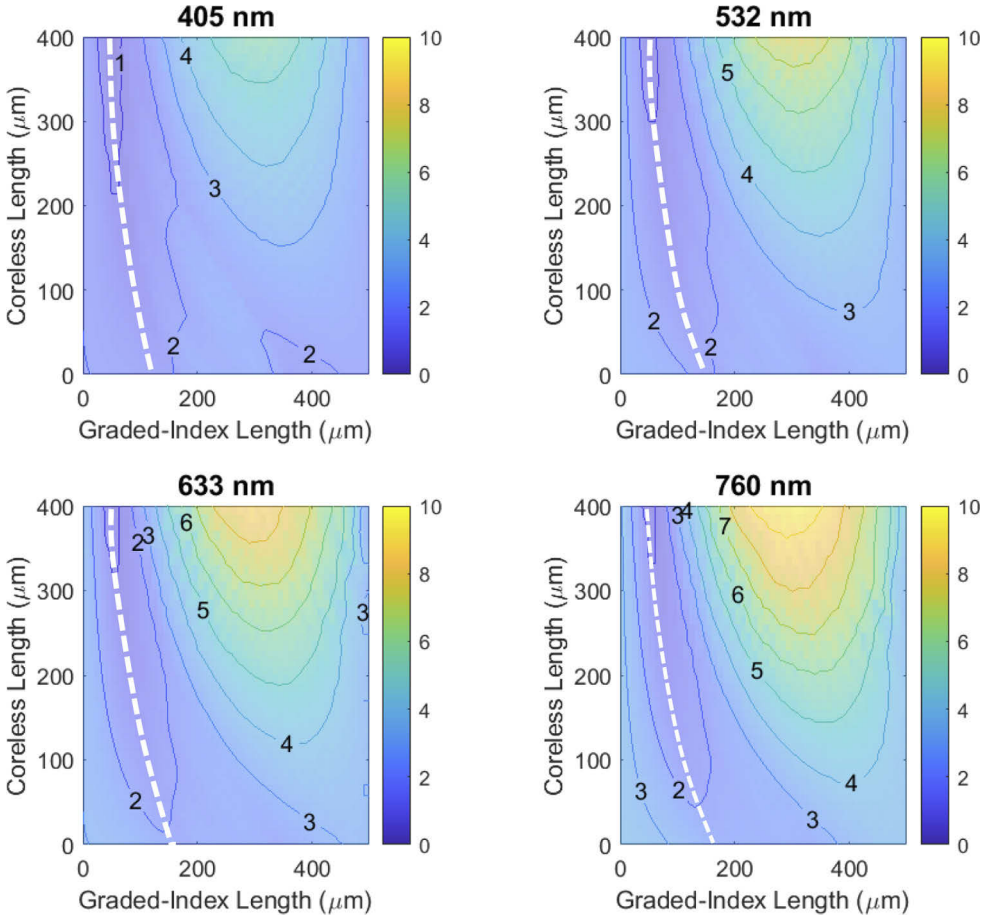

Fig. 6. The far-field divergence angle (FFDA) in degrees of the GIF tips as a function of graded-index and coreless fiber lengths for wavelengths in the visible from 405-760 nm.

there exists an optimal length at which the beam divergence is minimized. Beyond reaching this length the beam divergence increases again with a clear focal point observed.

Figure 9 demonstrates the case of a fixed 100-micron coreless length and varying graded-index fiber lengths. The simulation of the beam divergence is undertaken at a wavelength of 976 nm. The simulation again shows the variation in divergence, with the possibility of a focal point within the fiber. The simulations also demonstrate the periodic nature of the graded-index fiber.

In Fig. 10 the FFDA minima or troughs (<1°) from the contour plots of Fig. 6 and 7 are shown for several wavelengths and geometries considered. Figure 10 shows that for a given coreless fiber length, the longer the wavelength the longer the GIF length needs to be to ensure minimum FFDA. This relates to the wavelength dependence of the graded-index fiber pitch P_L (via the wavelength-dependence of $g(n_1,n_2, \lambda)$):

$$P_L(\lambda) = \frac{2\pi}{g} \tag{2}$$

Note that the period length of the graded-index lens for focusing or collimating Gaussian beams is ½ the pitch length [7]. In other words, periodic increases in the graded-index fiber length of ½ pitch in theory have no effect on performance.

Optics EXPRESS

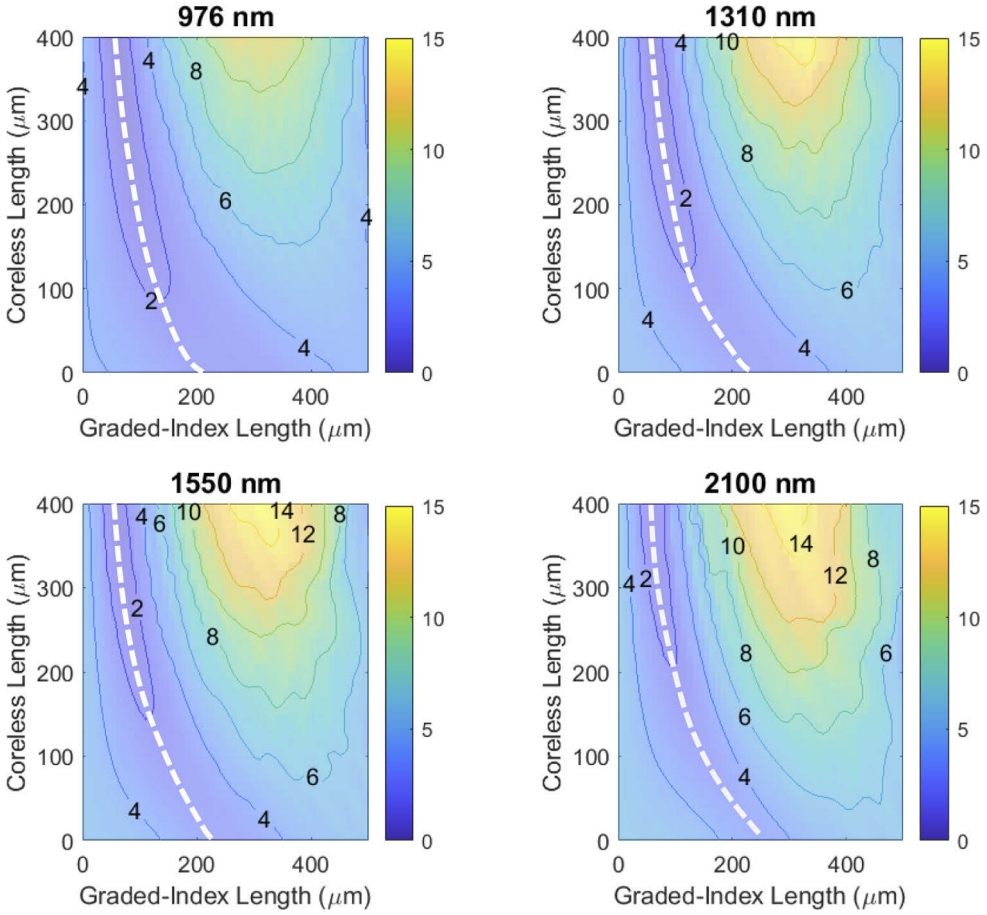

Fig. 7. The far-field divergence angle (FFDA) in degrees of the GIF tips as a function of graded-index and coreless fiber lengths for near-infrared to short-infrared wavelengths ranging from 976 - 2100 nm.

The graph also shows that for a given GIF length, the longer the wavelength, the longer the coreless length needs to be for reaching the minimum FFDA.

The troughs in the FFDA can be approximated by a third-order polynomial fit of the form:

$$L_C = aL_G^3 + bL_G^2 + cL_G + d \tag{3}$$

where L_c is the coreless fiber length, L_G is the graded-index fiber length and a, b, c and d are the coefficients of the polynomial fit. Units are in microns and the coefficients for several wavelengths are given in Table 1. These polynomial fits are valid in the regions simulated.

Figure 10 and the examples of Fig. 11 also show that to create broadband GIF tips the region of interest pertains to large coreless fiber and small graded-index fiber lengths. This is likely due to the greater expansion of the beam from the longer coreless fiber. A larger beam propagating through the graded-index fiber sees a larger change in refractive index due to the parabolic index profile shape which in turn increases the focusing strength of the graded-index fiber. The fits given in Eq. (3) provide easily-accessible guidelines for the design of collimating graded-index fiber tips optimized for low far-field divergence angle for several wavelengths. It is also worth noting that the beam size can be tailored without compromising the low divergence angle by simply selecting an appropriate point along the FFDA trough.

Optics EXPRESS

Figure 11(a) shows the beam divergence for a collimating GIF tip designed for broadband performance as per the red dashed region of Fig. 10. As can be seen the divergence angle is almost identical from 405 nm – 1550 nm. Figure 11(b) shows a design of a collimating GIF tip with high wavelength-dependence as seen by the large variation in beam divergence angle (i.e. black dashed region of Fig. 10).

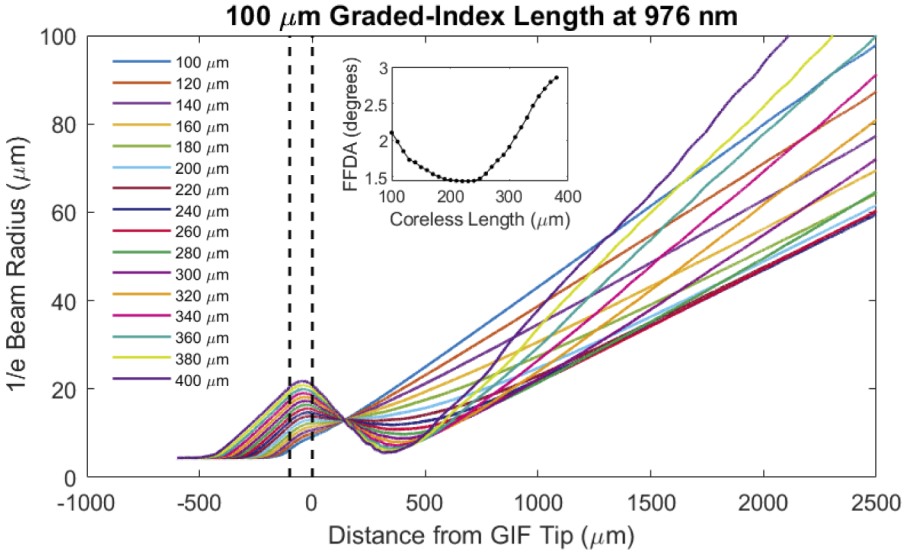

Fig. 8. Example of the 1/e beam radius of a GIF tip as a function of coreless fiber length (100-400 μm) with fixed graded-index length (100 μm). Inset shows the FFDA as function of the coreless fiber length. Wavelength assumed is 976 nm.

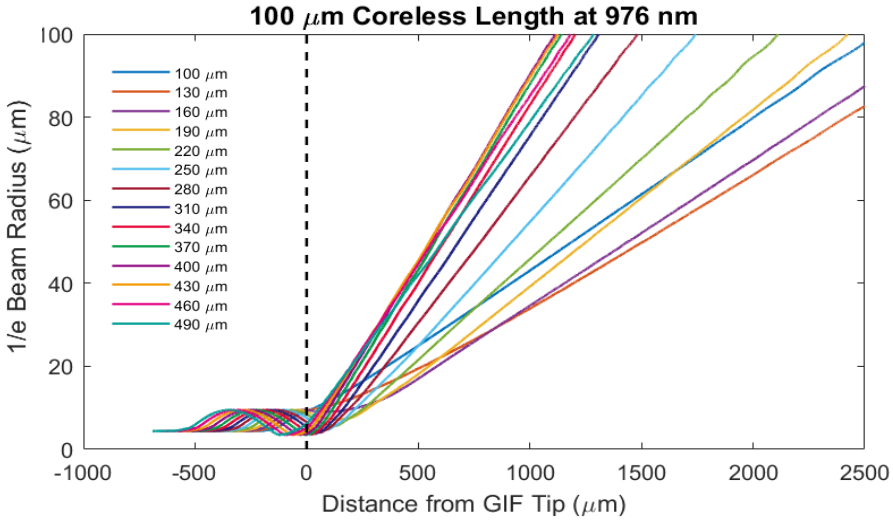

Fig. 9. Example of beam divergence of a GIF tip as a function of graded-index fiber length (100-490 μm) with fixed coreless fiber length (100 μm). Wavelength assumed is 976 nm.

Optics EXPRESS

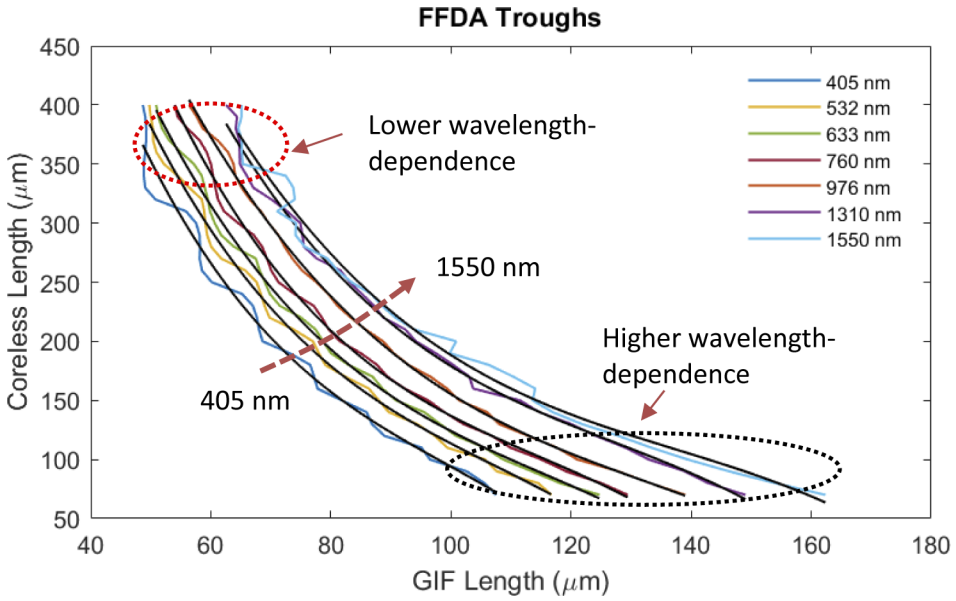

Fig. 10. Design guidelines for coreless and graded-index fiber lengths for minimizing the far-field divergence angle. Several wavelengths are shown.

Table 1. Third-order polynomial fit for FFDA troughs according to Eq. (3).

Wavelength (nm)	a x 10^{-3}	b	c	d
405	-0.9926	0.2953	-32.10	1343
532	-0.7578	0.2438	-28.67	1300
633	-0.6122	0.2125	-26.77	1288
760	-0.7302	0.2515	-31.06	1458
976	-0.4075	0.1628	-23.50	1285
1310	-0.5186	0.1984	-27.27	1440
1550	-0.3908	0.1615	-23.82	1346

2.3.3. Working distance for focusing probes

The collimation of light using an all-fiber probe has significant benefits in fiber-to-free-space applications. GIF tips have however more commonly been used and designed for imaging applications especially for OCT bioimaging. In such imaging applications the focal length determines the working distance and the spot size at the focus determines the resolution of the system. In this section we provide design guidelines for maximizing the working distance of GIF tips for imaging purposes. This is done for the first time, for a range of wavelengths spanning the UV to short-infrared. These studies could open the door to GIF tip imaging at a range of wavelengths outside of the typically used 1.3-micron OCT wavelength.

The working distance is defined/calculated from the distance between the fiber end face to the position of minimum waist. The location of the waist is determined using a change detection algorithm based on when the 1/e field radius is changing slopes. The change from a negative to positive slope indicates a minimum or waist in the beam. A change detection algorithm was used over a derivative based approach as it provided more stability in the location of the beam

Optics EXPRESS

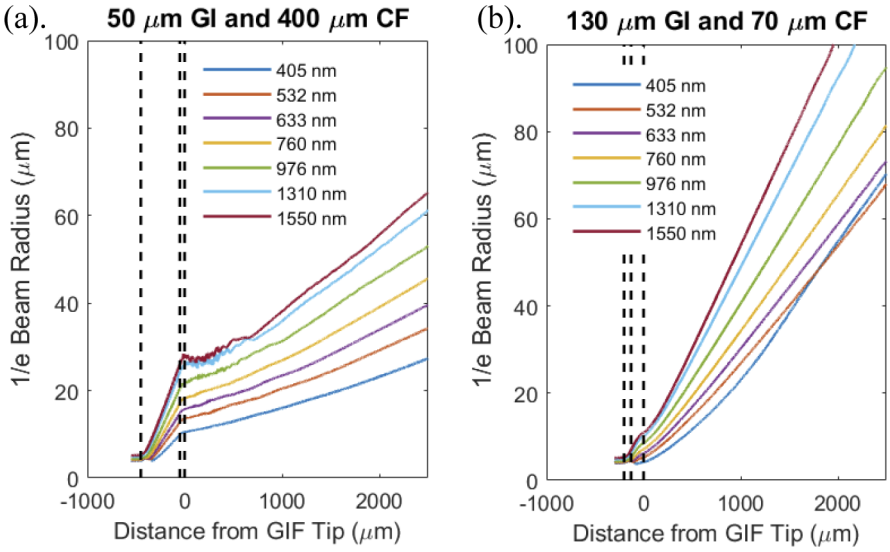

Fig. 11. Shown is the beam divergence for a GIF tip with (a) 50 µm graded-index and 400 µm coreless fiber lengths designed for broadband performance as per the red-dashed region in Fig. 10. Also shown is the beam divergence for a GIF tip with (b) 130 µm graded-index and 70 µm coreless fiber lengths in a wavelength-sensitive design as per the black highlighted region of Fig. 10.

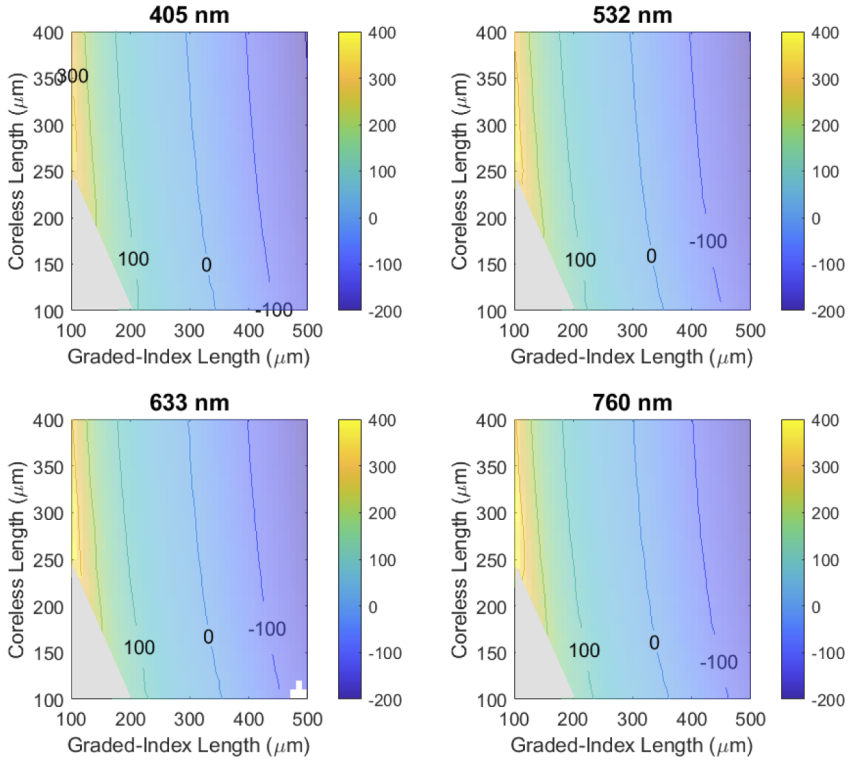

Fig. 12. The working distance (microns) of focusing GIF tips as a function of graded-index and coreless fiber lengths for UV and visible wavelengths ranging from 405 - 760 nm.

Optics EXPRESS

waist. Note that a negative value of the working distance indicates a focus occurring within the graded-index fiber.

Figures 12 and 13 provide graphs of the working distance as a function of coreless and graded-index fiber lengths. This is shown for the range of wavelengths considered. The graphs show that the working distance can be tuned by choice of coreless and graded-index fiber lengths. In particular the regions of short graded-index fiber length are optimal for increasing the working distance due to the weaker focusing strength as might be expected. Note that white regions are untrusted results stemming from issues with the simulations, whilst the grey shaded regions represent regions where there is no focus from the GIF tip. Note that no strong wavelength dependence is observed in this case likely because of the increase in focusing strength of the graded-index fiber segment which comes with longer wavelengths. The graphs provide easy-to-access design guidelines for creating GIF tips suited for imaging in the UV, visible or infrared.

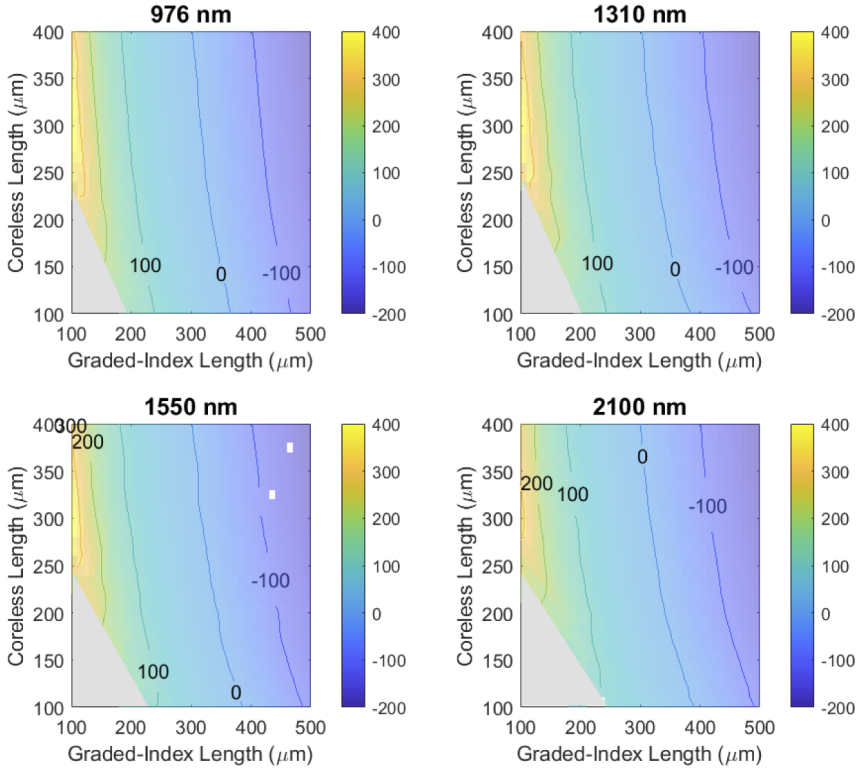

Fig. 13. The working distance (microns) of focusing GIF tips as a function of graded-index and coreless fiber lengths for near-infrared to short-infrared wavelengths ranging from 976 - 2100 nm.

3. Conclusions

In conclusion, we have provided an analysis and design guidelines for GIF tip probes for collimating and focusing the output of single-mode fiber. The numerical simulations covered a broad wavelength range spanning the UV to short-infrared, opening the door for these probes to be used in applications far beyond their conventional application in OCT imaging. Back-to-back or self-imaging collimating GIF tips could be used in a host of free-space to fiber coupled systems

Optics EXPRESS

without the requirement for bulk optics. The simulations in this paper have provided easily accessible guidelines to optimize such probes for various different applications.

Funding. Australian Research Council IDEAL Hub (IH150100028).

Acknowledgments. N. Riesen and D. G. Lancaster acknowledge financial support from ULVAC Inc., and the Australian Research Council Integrated Devices for End-User Analysis at Low Levels Research (IDEAL) Hub (IH150100028). N. P. acknowledges support from the Australian Government's Defence Science and Technology (DST) Group. The authors also acknowledge A/Prof Craig Priest and Dr Yongsop Hwang for feedback and suggestions.

Disclosures. The authors declare no conflicts of interest.

Data availability. The raw data underlying the results presented in this paper are not publicly available at this time but may be obtained from the authors upon reasonable request.

References

1. Y. Mao, S. Chang, S. Sherif, and C. Flueraru, "Graded-index fiber lens proposed for ultrasmall probes used in biomedical imaging," Appl. Opt. **46**(23), 5887–5894 (2007).
2. Y. Mao, S. Chang, S. Sherif, and C. Flueraru, "Fiber lenses for ultra-small probes used in optical coherent tomography," in *Advances In Biomedical Photonics And Imaging* (World Scientific, 2008), pp. 228–236.
3. Y. Mao, S. Chang, S. Sherif, and C. Flueraru, "Design and implementation of fiber lenses for ultra-small probes used in biomedical imaging," in *Optics in Health Care and Biomedical Optics III*, (International Society for Optics and Photonics, 2008), 68261A.
4. E. Swanson, C. L. Petersen, E. McNamara, R. B. Lamport, and D. L. Kelly, "Ultra-small optical probes, imaging optics, and methods for using same," (Google Patents, 2002).
5. M. S. Jafri, S. Farhang, R. Tang, N. Desai, P. S. Fishman, R. G. Rohwer, C.-M. Tang, and J. M. Schmitt, "Optical coherence tomography in the diagnosis and treatment of neurological disorders," J. Biomed. Opt. **10**(5), 051603 (2005).
6. C. Gomez-Reino, M. V. Perez, C. Bao, and M. T. Flores-Arias, "Design of GRIN optical components for coupling and interconnects," Laser Phot. Rev. **2**(3), 203–215 (2008).
7. C. Wang, C. Fang, Z. Tang, Y. Yu, Y. Mao, and B. Qi, "Analytical method for designing gradient-index fiber probes," Opt. Eng. **50**(9), 094202 (2011).
8. X. Sun and J. Li, "Design of a long working distance graded index fiber lens with a low NA for fiber-optic probe in OCT application," in *Optical Fibers and Sensors for Medical Diagnostics and Treatment Applications XIV*, (International Society for Optics and Photonics, 2014), 89380B.
9. S. Bi, C. Wang, J. Zhu, Z. Yuan, Y. Yu, S. Valyukh, and A. Asundi, "Influence of no-core fiber on the focusing performance of an ultra-small gradient-index fiber probe," Opt. Lasers Eng. **107**, 46–53 (2018).
10. M. Van Buren and N. A. Riza, "Foundations for low-loss fiber gradient-index lens pair coupling with the self-imaging mechanism," Appl. Opt. **42**(3), 550–565 (2003).
11. D. Lorenser, X. Yang, and D. D. Sampson, "Accurate modeling and design of graded-index fiber probes for optical coherence tomography using the beam propagation method," IEEE Phot. J. **5**(2), 3900015 (2013).
12. M. Zickar, W. Noell, C. Marxer, and N. de Rooij, "MEMS compatible micro-GRIN lenses for fiber to chip coupling of light," Opt. Express **14**(10), 4237–4249 (2006).
13. N. Riesen, N. Phillips, C. Priest, L. V. Nguyen, S. C. Warren-Smith, and D. G. Lancaster, "Design considerations for graded index fiber tip Fabry-Perot interferometers," Meas. Sci. Technol. **32**(5), 055201 (2021).
14. N. Riesen, N. Phillips, C. Priest, L. V. Nguyen, and D. G. Lancaster, "Lensed GRIN fiber-optic Fabry-Perot interferometers," in *Frontiers in Optics*, (Optical Society of America, 2020), JTu7D. 4.
15. B. Du, X. Xu, J. He, K. Guo, W. Huang, F. Zhang, M. Zhang, and Y. Wang, "In-Fiber collimator-based Fabry-Perot interferometer with enhanced vibration sensitivity," Sensors **19**(2), 435 (2019).
16. T. K. Gangopadhyay, "Non-contact vibration measurement based on an extrinsic Fabry–Perot interferometer implemented using arrays of single-mode fibres," Meas. Sci. Technol. **15**(5), 911–917 (2004).
17. H. Fukano and K. Yoshioka, "Fabry-Perot Optical Fiber Temperature Sensor using Graded-Index Fiber for Cryotherapy," in *2019 24th Microoptics Conference (MOC)*, (IEEE, 2019), 236–237.
18. K. K. Gill, N. Riesen, C. Priest, N. Phillips, B. Guan, and D. G. Lancaster, "On-chip absorption spectroscopy enabled by graded index fiber tips," Biomed. Opt. Express **12**(1), 181–190 (2021).
19. P. Hofmann, A. Mafi, C. Jollivet, T. Tiess, N. Peyghambarian, and A. Schulzgen, "Detailed investigation of mode-field adapters utilizing multimode-interference in graded index fibers," J. Lightw. Technol. **30**(14), 2289–2298 (2012).
20. Y. Gong, A.-Y. Ye, Y. Wu, Y.-J. Rao, Y. Yao, and S. Xiao, "Graded-index fiber tip optical tweezers: Numerical simulation and trapping experiment," Opt. Express **21**(13), 16181–16190 (2013).
21. Y. Mao, S. Chang, S. Sherif, and C. Flueraru, "Fiber probes used in optical coherence tomography," in *Photonics North 2008*, (International Society for Optics and Photonics, 2008), 70990A.
22. J. Lee, "Collimation scheme for fiber lens using polymer coating," in *2012 7th International Conference on Computing and Convergence Technology (ICCCT)*, (IEEE, 2012), 1423–1425.
23. C. Wang, T.-t. Xu, S.-b. Bi, X. Mao, J. Zhu, and Z.-w. Yuan, "Measurement of the focusing constant of gradient-index fiber lens and its application in developing GRIN fiber probes," Meas. **90**, 542–548 (2016).

Optics EXPRESS

24. R. Kasztelanic, A. Filipkowski, A. Anuszkiewicz, P. Stafiej, G. Stepniewski, D. Pysz, K. Krzyzak, R. Stepien, M. Klimczak, and R. Buczynski, "Integrating free-form nanostructured GRIN microlenses with single-mode fibers for optofluidic systems," Sci. Rep. **8**(1), 5072 (2018).
25. C. Wang, S. Bi, X. Xia, and Y. Yu, "Further analysis of focusing performance of an ultra-small gradient-index fiber probe," Opt. Eng. **53**(1), 013106 (2014).
26. W. Chi, M. You-Xin, T. Zhi, F. Chen, Y. Ying-Jie, and Q. Bo, "Numerical simulation of a gradient-index fibre probe and its properties of light propagation," Chinese Phys. B **20**(11), 114218 (2011).
27. X. Wang, J. Fu, X. Liu, and L.-M. Tong, "Subwavelength focusing by a micro/nanofiber array," J. Opt. Soc. Am. A **26**(8), 1827–1833 (2009).
28. S.-S. Wang, J. Fu, M. Qiu, K.-J. Huang, Z. Ma, and L.-M. Tong, "Modeling endface output patterns of optical micro/nanofibers," Opt. Express **16**(12), 8887–8895 (2008).
29. V. Shinoj, V. Murukeshan, S. Tor, N. Loh, and S. Lye, "Design, fabrication, and characterization of thermoplastic microlenses for fiber-optic probe imaging," Appl. Opt. **53**(6), 1083–1088 (2014).
30. D. Lorenser, X. Yang, R. Kirk, B. Quirk, R. McLaughlin, and D. Sampson, "Ultrathin side-viewing needle probe for optical coherence tomography," Opt. Lett. **36**(19), 3894–3896 (2011).
31. W. Jung, W. A. Benalcazar, A. Ahmad, U. Sharma, H. Tu, and S. A. Boppart, "Numerical analysis of gradient index lens-based optical coherence tomography imaging probes," J. Biomed. Opt. **15**(6), 066027 (2010).
32. E. Bélanger, J.-P. Bérubé, B. de Dorlodot, P. Marquet, and R. Vallée, "Comparative study of quantitative phase imaging techniques for refractometry of optical waveguides," Opt. Express **26**(13), 17498–17510 (2018).
33. I. Malitson, "Interspecimen comparison of the refractive index of fused silica," JOSA **55**(10), 1205–1209 (1965).
34. FEMSIM Guide, "RSoft Inc., 200 Executive Blvd," Ossining, NY 10562(2001).
35. BEAMPROP Guide, retrieved: https://www.synopsys.com/photonic-solutions/rsoft-photonic-device-tools/passive-device-beamprop.html (Accessed May 2021)
36. S. Gross, N. Riesen, J. D. Love, and M. J. Withford, "Three-dimensional ultra-broadband integrated tapered mode multiplexers," Las. Phot. Rev. **8**(5), L81–L85 (2014).